Effects of Process Parameters on the Weld Quality During Double-Pulsed Gas Metal Arc Welding of 2205 Duplex Stainless Steel

Yu Hu and Jiaxiang Xue

Abstract In this paper, double-pulsed melting inert-gas welding (MIG) was conducted on 2205 duplex stainless steel and the effects of the number of strong pulses, the number of weak pulses and the welding speed were studied. The electrical parameters in the welding process were collected through the wavelet analyzer. The waveform charts of the current and voltage, the U-I diagram, the energy input, the dynamic resistance and other real-time signals were analyzed. In addition, mechanical tensile and metallographic tests were conducted. The results demonstrated that the welding speed had the highest impact on the welding quality among all the three factors, followed by the number of weak pulses and the number of strong pulses. The welded seam obtained by various numbers of strong and weak pulses was relatively uniform, indicating that the effect of the number of strong and weak pulses on the welded seam was relatively low. The tensile fracture occurred in the base material part of the duplex stainless steel, indicating that the welded seam region had a higher tensile strength than the base material. The tensile strengths of various specimens were similar. When the welding speed was reduced, the heat input increased during the welding of the welded seam, the cooling rate of the welded seam slowed down, whereas the ferrite transition duration increased, which led to the formation of higher amount of austenite and a relatively coarse structure.

Keywords Duplex stainless steel · Double pulse · MIG · Welding quality

1 Introduction

Duplex Stainless Steels (DSS) combine the excellent toughness and weldability of austenitic stainless steels and the high strength and resistance against the oxide stress corrosion of the ferritic stainless steel. Therefore, the DSS display the merits

Y. Hu · J. Xue (✉)
School of Mechanical and Automotive Engineering, South China University of Technology, Guangzhou 510641, China
e-mail: mejiaxue@scut.edu.cn

S. Chen et al. (eds.), *Transactions on Intelligent Welding Manufacturing*,
Transactions on Intelligent Welding Manufacturing,
https://doi.org/10.1007/978-981-10-8330-3_7

of good resistance against pitting, crevice corrosion, stress corrosion and corrosion fatigue, exhibiting corrosion resistance, good comprehensive mechanical properties and other characteristics. Therefore, the application of DSS has rapidly been developed and it is widely utilized in petroleum, chemical, marine and power industries [1, 2].

Although the TIG welding can acquire the fish-scale appearance, the corresponding production efficiency is low. Consequently, it is difficult to meet the requirements of large-scale production. The pulse MIG welding has higher production efficiency and is easy for automated production to be achieved, whereas certain issues exist in the welding quality [3, 4]. The current significantly advanced welding methods include the pulsed melting inert gas welding (P-MIG), the double wire melting argon arc welding, the alternating current pulsed melting inert gas welding (AC-PMIG), the double-pulsed gas metal arc welding (DP-GMAW) and the friction stir welding. The MIG welding process through the double pulse is the utilization of a low-frequency signal to modulate the high-frequency pulse current, in order for the current waveform chart the present an alternative appearance of the strong pulse and weak pulse groups. Such a welding method not only has the characteristics of single-pulse welding such as the low average input current, whereas it also stirs the molten pool and releases the bubbles, resulting in the fish-scale weld seam. At present, the domestic and international studies on the double-pulsed MIG mainly are focused on the arc behavior, the welding speed, the joint performance and the post-treatment subsequently to welding [5]. In contrast, the researches on the effects of the number of strong and weak pulses and the welding speed on the welding process for stainless steels are rarely reported. In order to understand the effects of the number of both double pulse and welding speed on the welded seam shaping, the MIG welding was performed on a 2205 duplex stainless steel through various numbers of strong and weak pulses. The pulse number effects on the formation, the welding stability and the mechanical properties and microstructure of the welded seam were investigated, providing reference to the processing parameters selection in the double-pulsed welding of duplex stainless steels [6, 7].

2 Test Methods

2.1 Test Material

The test material utilized in the test was a 4.0 mm-thick duplex stainless-steel plate. The ER2209 welding wire with of 1.2 mm in diameter was selected. The chemical compositions of these two materials are presented in Table 1.

Table 1 Chemical composition of 2205 and ER2209

Element	C	Mn	Si	Cr	Ni	Mo	N	S	P
2205	0.024	1.4	0.62	21.3	5.4	3.0	0.16	0.01	0.024
ER2209	0.017	1.73	0.52	22.43	8.45	2.94	0.15	0.008	0.012

2.2 Test Platform

The data acquisition platform for the welding test included a load resistance box, an industrial personal computer (Advantech 610), a data acquisition card (Advantech PCL 1800), a Huawei automatic walking control device, an arc dynamic wavelet analyzer for the real-time signals acquisition of the voltage and current, a soft switching inverter based on the digital signal processing (DSP) for pulsed MIG welding, a wire feeding machine and other devices.

2.3 Process and Parameters

The self-developed digital multi-functional power supply was adopted in the test. A welding arc dynamic wavelet analyzer was utilized to measure the voltage and the current. The arc dynamic wavelet analyzer was an important tool to collect and analyze the real-time signal during welding. The corresponding host computer software was installed on the industrial personal computer to collect the real-time current and voltage signals during welding. Following the analysis and processing, the signals could be utilized to determine the welding stability. Prior to welding, the oxide film on the base metal surface was polished with the No. 800 grit sandpaper, whereas the grease residue on the base metal surface was cleaned with acetone.

An orthogonal test table was designed based on the number of strong pulses, the number of weak pulses and the welding speed, as presented in Table 2. Respectively, the numbers of strong pulses were 10, 12, 14 and 16; the numbers of weak pulses were 5, 6, 7 and 8; the welding speeds were 0.6, 0.8, 1.0 and 1.2 m/min. The peak and base current of the strong pulse group were 440 and 110 A; the peak and base current of the weak pulse group were 280 and 70 A. The protective gas was argon (Ar) with the purity of 99.99% and the flow rate of 18 L/min. The welding object was the duplex stainless-steel plate with the thickness of 4 mm and the surfacing welding was executed.

Table 2 Orthogonal test table

No.	No. of strong pulses N_1	No. of weak pulses N_2	Welding speeds (m/min)
1	10	5	0.6
2	10	6	0.8
3	10	7	1.0
4	10	8	1.2
5	12	5	0.8
6	12	6	0.6
7	12	7	1.2
8	12	8	1.0
9	14	5	1.0
10	14	6	1.2
11	14	7	0.6
12	14	8	0.8
13	16	5	1.2
14	16	6	1.0
15	16	7	0.8
16	16	8	0.6

3 Test Result and Analysis

3.1 Appearance of Welded Seam

According to the welding quality and uniformity of the welded seam, the comprehensive evaluation indicator, A, and three subordinate evaluation indicators: A1 (welding stability), A2 (with or without arc breaking) and A3 (with or without splash) were determined. According to the fuzzy comprehensive evaluation model, the synthesis product with fuzzy relation and the matrix could be obtained as: $S = A{*}R{\cdot}F$ [8], where A is the indicator weight as estimated by experts, $A = (A1, A2, A3) = (0.8, 0.15, 0.05)$. According to the principle of difference scoring method, the Vij ($j = 1, 2, 3$) was differentially scored. The evaluation set was $F = (f1, f2, f3)T = (100, 75, 50)T$. The evaluation on every test indicator is carried out by the group composed of five experts. As an example, the comprehensive evaluation matrix for the index A1 of weld seam in test 1 was $V1 = (V11, V12, V13) = (0.4, 0.2, 0.4)$, the $V2$ and $V3$ can be obtained according to the same principle. The comprehensive score was calculated as $S1 = A1{*}R1{\cdot}F = 76$. Similarly, the other test scores could be obtained. The evaluation table of the experts is presented as Table 3.

All tests, based on the parameters in Table 2, could be successfully completed and the formed welded seams were continuous and uniform. The undercut and any other defects were seldom observed. With reference to the orthogonal test table, it could be observed from the seam images that the welded surface formed in test 1

Table 3 Evaluation table given by experts

Stability A_1			Arc breaking A_2			Splash A_3			Comprehensive score for A
Stable	Common	Poor	No	Common	Obvious	No	Common	Obvious	
V_{11}	V_{12}	V_{13}	V_{21}	V_{22}	V_{23}	V_{31}	V_{32}	V_{33}	
2	1	2	3	1	1	2	2	1	76
2	1	2	2	1	2	2	1	2	72
2	2	1	3	1	1	2	2	1	82
2	1	2	1	2	2	3	0	2	74
2	2	1	2	2	1	3	1	1	78
2	1	2	2	2	1	2	2	1	75
1	3	1	2	2	1	2	1	2	74
4	1	0	2	2	1	3	1	1	80
4	1	0	3	1	1	3	1	1	85
1	2	2	2	1	2	3	1	1	73
3	0	2	1	2	2	3	1	1	81
3	1	1	3	1	1	1	2	2	78
1	1	3	1	1	3	2	0	3	72
1	2	2	1	0	4	2	1	2	71
2	2	1	2	2	1	1	3	1	76
3	1	1	2	2	1	3	1	1	77

was smooth; without an apparent fish-scale pattern; the edge of the weld was not significantly flat. Therefore, the score given by the evaluation system was approximately 76 points. The welding in test 9 was quite stable, with less splashing and displayed the best quality of the weld. The two sides of the welded seam were flat and uniform, whereas a fish-scale weld groove could be observed. The splashing in welding process 2 was less, whereas the welded seam width was inconsistent. An apparent snake-shaped pattern appeared and the fish-scale pattern was not observed. Following the orthogonal test data processing (Table 4), it could be concluded that among the number of strong pulses, the number of weak pulses and the welding speed, the welding speed had the highest impact on the weldment quality. The weldments are presented in Fig. 1.

3.2 Analysis on Real-Time Data Acquired During Welding

Waveform chart of current

The test 9 with the improved welding quality was selected as the real-time data analysis object. The real-time current signal acquired during welding is presented in Fig. 2. Figure 2a, b are the waveform charts of the current. The current waveform in the entire welding process was well reproducible and no instantaneous burr was

Table 4 Orthogonal test results

Test No.	Number of strong pulses N_1	Number of weak pulses N_2	Welding speeds (m/min)	Comprehensive score
1	10	5	0.6	76
2	10	6	0.8	72
3	10	7	1.0	82
4	10	8	1.2	74
5	12	5	0.8	78
6	12	6	0.6	75
7	12	7	1.2	74
8	12	8	1.0	80
9	14	5	1.0	85
10	14	6	1.2	73
11	14	7	0.6	81
12	14	8	0.8	78
13	16	5	1.2	72
14	16	6	1.0	71
15	16	7	0.8	76
16	16	8	0.6	77
Average k_1	76.00	77.75	77.25	
Average k_1	76.75	72.75	76.0	
Average k_1	79.25	78.25	79.5	
Average k_1	74.0	77.25	73.25	
Range, R	5.25	5.5	6.25	
Order	Welding speed > Number of weak pulses > Number of strong pulses			

present. The statistical average current was 200 A; the base current of the strong pulse group was 110 A and the peak current was 440 A; the peak current of the weak pulse group was 280 A and the base current was 70 A.

Voltage waveform chart

The arc length stability in the welding process directly represents the voltage stability. Figure 3a presents the waveform chart of the welding voltage. The statistical average voltage was 26.27 V, with the minimum voltage of 17.79 V and the maximum voltage of 38.66 V. The entire waveform appeared to change regularly. The lower oscillation range of the voltage indicated a stable welding. Figure 3b presents the amplified waveform of the voltage. It could be observed that the voltage became higher subsequently formed a peak when the current approached the corresponding peak, which corresponded to the arc length sudden elongation

(a) welded seam formed during test 1

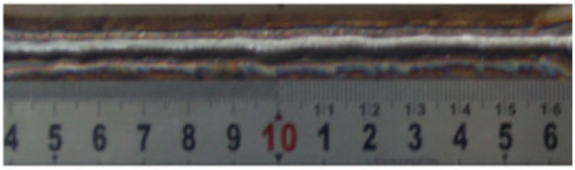

(b) welded seam formed during test 2

(c) welded seam formed during test 3

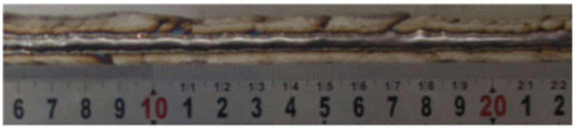

(d) welded seam formed during test 4

(e) welded seam formed during test 5

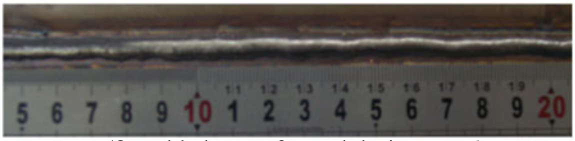

(f) welded seam formed during test 6

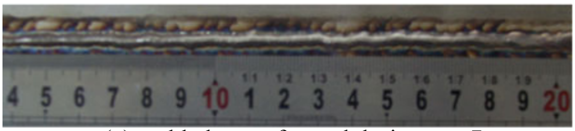

(g) welded seam formed during test 7

Fig. 1 Welded seams formed during orthogonal test

(h) welded seam formed during test 8

(i) welded seam formed during test 9

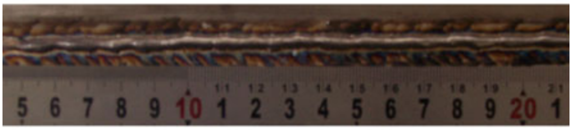

(j) welded seam formed during test 10

(k) welded seam formed during test 11

(l) welded seam formed during test 12

(m) welded seam formed during test 13

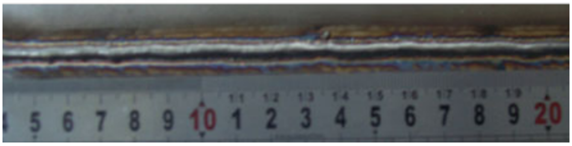

(n) welded seam formed during test 14

Fig. 1 (continued)

(o) welded seam formed during test 15

(p) welded seam formed during test 16

Fig. 1 (continued)

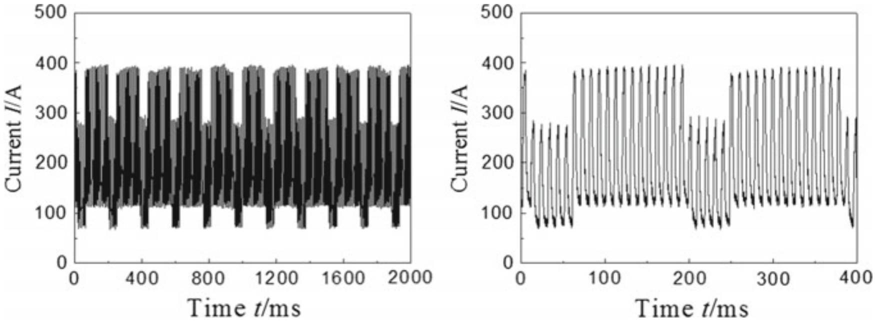

(a) waveform chart of current (b) amplified waveform chart of current

Fig. 2 Real-time signal of current during welding

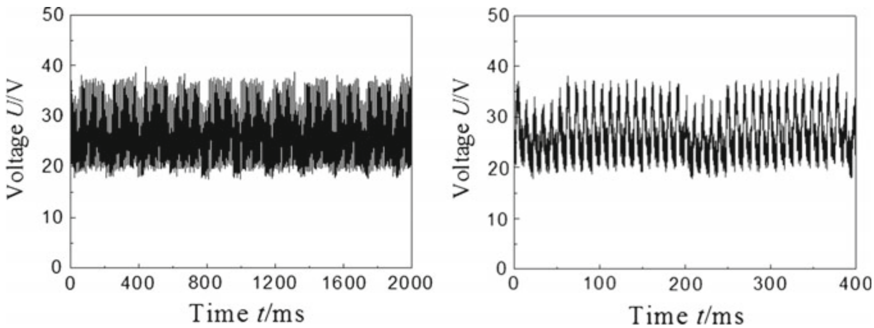

(a) waveform chart of voltage (b) amplified waveform chart of voltage

Fig. 3 Real-time voltage signal during welding following the melt droplet transition. In contrast, in the pilot arc base current stage, the voltage was relatively low and stable, with lower oscillations.

U-I diagram

Figure 4 presents the U-I diagram of the welding process, the abscissa represented the current during welding and the ordinate displayed the voltage corresponding to the current, as a combination of Figs. 2 and 3. From the U-I diagram the dynamic welding could be analyzed and evaluated, intuitively. The edge lines drawn by the current and the voltage were clear and neat, along with centralized distribution, which indicated that the current and the voltage during welding were concentrated in a relatively narrow range and without high jumps. Consequently, the entire welding displayed a good stability.

Input energy of welding and dynamic resistance

The input energy of the welding, presented in Fig. 5, is the product of the instantaneous current and instantaneous voltage of the arc, which determined the

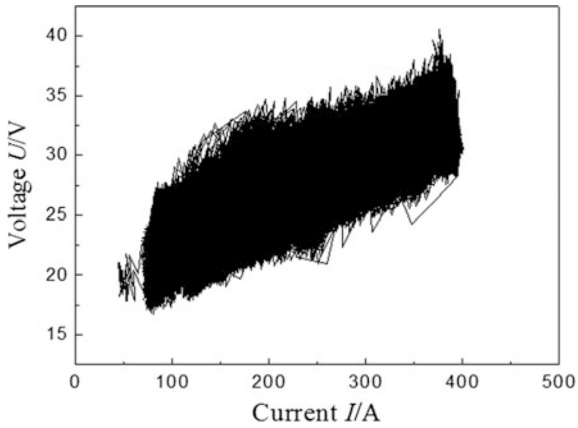

Fig. 4 U-I diagram of welding

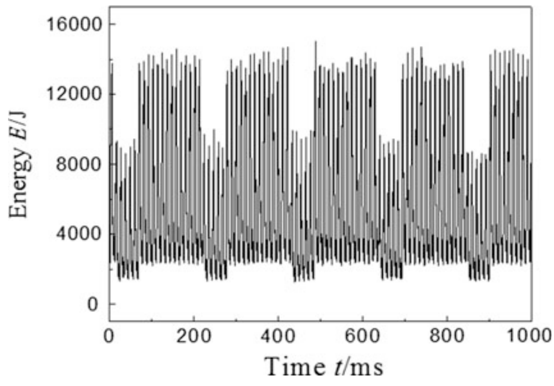

Fig. 5 Input energy of welding process

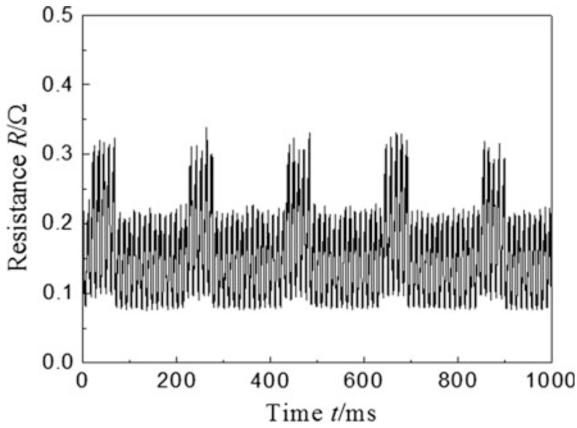

Fig. 6 Dynamic resistance

arc length and the transition form of the droplet [9–12]. As it could be observed, the pulse energy waveform displayed a regular rectangular change, indicating that the droplet transition during welding was regular. Figure 6 presents the dynamic resistance during welding, which was the ratio of the instantaneous voltage and current. It could be observed that the resistance fluctuated within the 0.1–0.3 Ω range around the 0.2 Ω, indicating a good concentration and regularity. From the welding tests, the entire welding was successfully complete and no arc breaking or short circuit phenomena were observed.

3.3 Analysis on Mechanical Properties of Welded Seam

The surfaces of the specimen following welding were polished and the tensile specimens were prepared through wire cutting. The thickness of the specimens was 4 mm. The tensile test result of the welded seams is presented in Table 5. The fracture position occurred in base material part of the duplex stainless steel, indicating that the welded seam had a higher tensile strength than the base material. The difference in the tensile strength of various samples was not significantly high, which was consistent with the aforementioned conclusion that the fracture occurred in the base metal part rather than the fusion and the heat-affected zones.

3.4 Metallographic Analysis of Welded Seam

The weld seams in test 9 had improved welding quality and were consequently selected as the analysis objects in the metallographic analysis. The welded seam could be divided into three zones: the molten pool zone, the fusion zone and the heat-affected zone. The microstructures of the fusion zone observed with the

Table 5 Tensile strength of welded seam

Test no.	No. of strong pulses N_1	No. of weak pulses N_2	Speed (m/min)	Tensile strength (MPa)	Fracture position
1	10	5	0.6	903.12	Lower region of base material
2	10	6	0.8	857.3	Upper region of base material
3	10	7	1.0	859.66	Lower region of base material
4	10	8	1.2	850.42	Upper region of base material
5	12	5	0.8	868.47	Upper region of base material
6	12	6	0.6	873.91	Lower region of base material
7	12	7	1.2	863.31	Upper region of base material
8	12	8	1.0	865.43	Lower region of base material
9	14	5	1.0	861.84	Lower region of base material
10	14	6	1.2	863.15	Lower region of base material
11	14	7	0.6	889.21	Lower region of base material
12	14	8	0.8	870.04	Lower region of base material
13	16	5	1.2	873.86	Lower region of base material
14	16	6	1.0	872.42	Lower region of base material
15	16	7	0.8	887.05	Lower region of base material
16	16	8	0.6	904.86	Upper region of base material

50-fold and 500-fold microscope are presented in Figs. 7 and 8, respectively. The microstructure had an irregular strip feature and an alternating distribution of two phases, such as the substrate was ferrite whereas the strip, lump and feathery organizations were austenite. The molten pool zone, presented in Fig. 9, demonstrated the as-cast dendritic crystal structure that was mainly composed of the austenite structure. The precipitates of high-sized tracts of feathery and dendritic austenite were observed, indicating that the metal in the molten pool had poorer hardness and toughness, along with increased brittleness. The microstructure of the base metal is presented in Fig. 10. The structure had a clear orientation and a

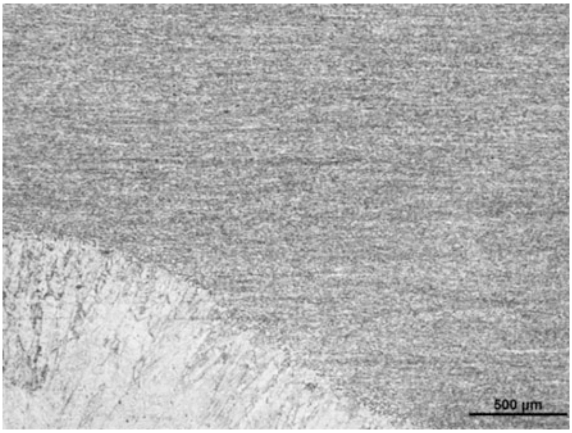

Fig. 7 Metallographic image of fusion zone (50 ×)

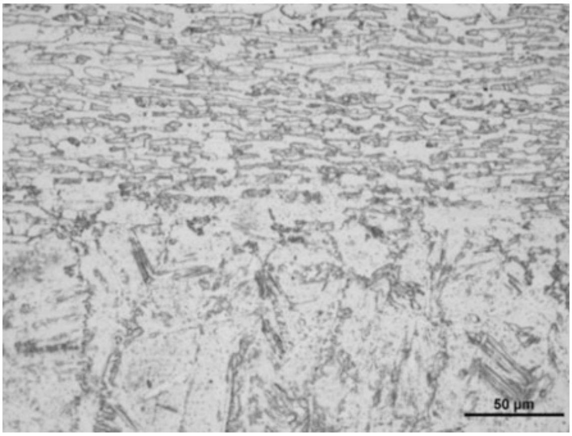

Fig. 8 Metallographic image of fusion zone (500 ×)

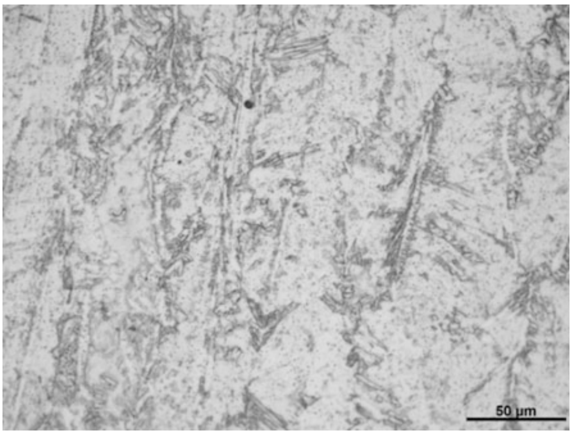

Fig. 9 Metallographic image of molten pool (500 ×)

strip-like distribution. The strip-like austenite distributed on the ferrite substrate and the proportions of the two components were similar. The darker part was the ferrite, whereas the lighter part was the austenite. The microstructure of the heat-affected zone is presented in Fig. 11, where the grains were not significantly coarsened, still belonging to the typical dual-phase morphology of the austenite and ferrite.

The metallographic graphs of the molten pool zones in tests 1, 6, 9, and 13 are presented in Figs. 12, 13, 9 and 14, whereas the corresponding welding speeds were 0.6, 0.8, 1.0 and 1.2 m/min, respectively. As it could be observed from these figures, as the welding speed decreased, the heat input during welding increased and the cooling rate of the welded seam became slower, increasing the transition duration and promoting the formation of austenite, resulting in a relatively coarse structure.

Fig. 10 Metallographic image of base material (500 ×)

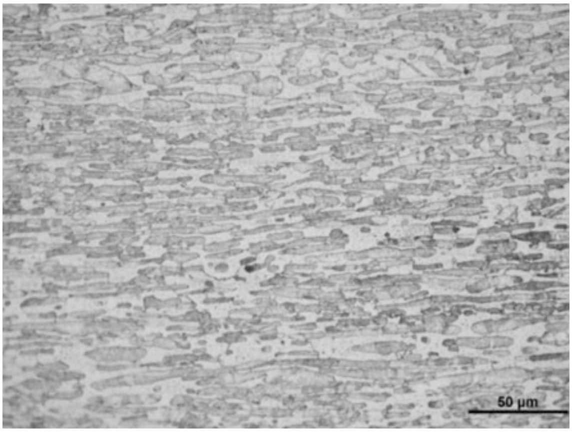

Fig. 11 Metallographic image of HAZ (500 ×)

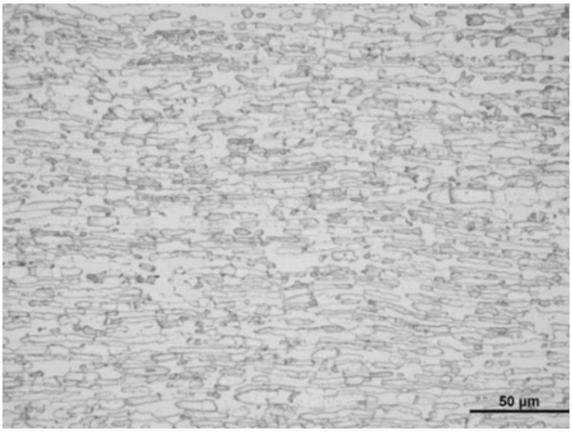

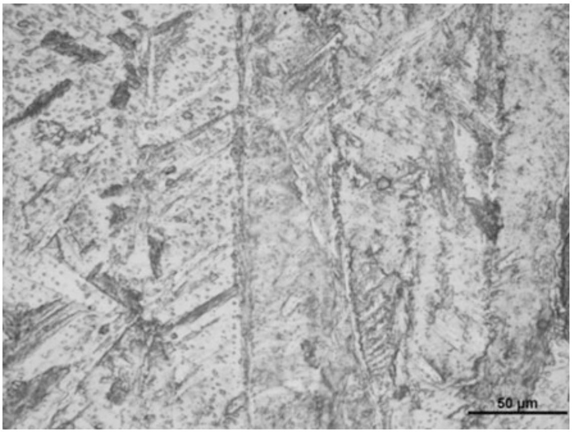

Fig. 12 Metallographic image of molten pool (500 ×)

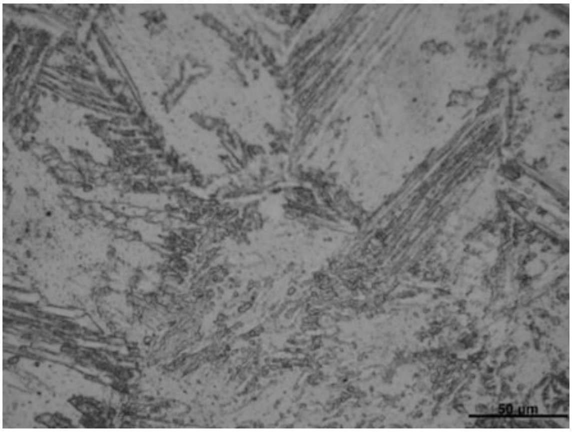

Fig. 13 Metallographic image of molten pool (500 ×)

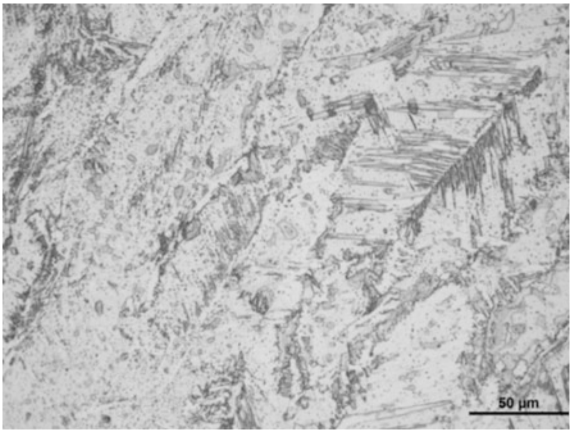

Fig. 14 Metallographic image of molten pool (500 ×)

4 Conclusion

(1) During the welding tests of the 4 mm-thick duplex stainless-steel plate, the welding was smooth and the splashes were less. The welded seam was good in appearance, displaying uniform and bright fish-scale morphology. The arc voice was soft and no melting penetration phenomenon was observed.
(2) Among the aforementioned three factors, the order in affecting extent was weld speed > number of weak pulses > number of strong pulses. The welded seams obtained under various numbers of strong and weak pulses were relatively uniform, indicating that the number of strong and weak pulses only had a slight effect on the welded seam.
(3) The tensile fracture occurred in the base material part of the duplex stainless steel, indicating that the welded seam had a higher tensile strength than the base metal, whereas the difference in the sample tensile strengths was insignificant.
(4) As the welding speed decreased, the input heat during welding increased and the cooling rate of the welded seam became slower, increasing the transition duration of ferrite and promoting the formation of higher amount of austenite, resulting in a relatively coarse structure.

Acknowledgements The research was sponsored by the High-level Leading Talent Introduction Program of GDAS (2016GDASRC-0106), the Natural Science Foundation of Guangdong (2016A030313117), the Industry-university-research of Guangdong province and Ministry of Education (2013B090600098).

References

1. Wang Z, Xu H, Wu W et al (2011) Joint performance of duplex stainless 2205 by laser MIG hybrid welding. Trans China Weld Inst 32(2):105–108
2. Wang Z, Han J, Song H et al (2011) Comparative analysis for joint performance of duplex stainless steel by different arc welding methods. Trans China Weld Inst 32(4):37–40
3. Yao P, Jiaxiang Xue, Qiang Zhu et al (2014) Quantitative evaluation of double wire pulsed welding stability based on probability density distribution. Trans China Weld Inst 35(7):51–54
4. Yao P, Xue J, Zhong L et al (2012) Intelligent process expert database of double pulse MIG welding of Al-Si alloy. Trans China Weld Inst 21(1):59–63
5. Xie H, Wang L, Sha X et al (2015) Analysis of strong and weak pulse ratio on weld quality of AA6061 aluminum alloy double pulsed gas metal arc welding. Trans China Weld Inst 36 (12):77–80
6. Yoganandh J, Kannan T, Kumaresh Babu SP et al (2013) Optimization of GMAW process parameters in austenitic stainless-steel cladding using genetic algorithm based computational models. Exp Tech 37(5):48–58
7. Chen H, Xue J, Heng G (2016) Improvement of double wire mig welding by using sine wave pulse modulation control method. In: IHMSC-2016 eighth international conference on intelligent human-machine systems and cybernetics, pp 451–455
8. Zhu Q, Xue J, Xu M (2015) A probe into backward median current waveform welding of aluminum alloys. J S China Univ Technol (Natural Science Edition) 43(3):15–20

9. Zhu Q, Xue J, Xu M (2016) Gaussian pulsed MIG welding of aluminum alloy sheet. Trans China Weld Inst 37(8):71–74
10. Niu Y, Xue H, Li H (2012) Effect of peak pulse voltage on metal transfer and formation of weld in double-wire pulsed MIG welding. Trans China Weld Inst 31(1):50–54
11. Aktepe A, Ersöz S, Lüy M (2014) Welding process optimization with artificial neural network applications. Neutral Netw World 24(6):655–670
12. Wang LL, Wei HL, Xue JX et al (2017) A pathway to microstructural refinement through double pulsed gas metal arc welding. Scripta Mater 134:61–65